PROCEEDINGS OF SCIENCE

Investigating starburst-driven neutrino emission from GOALS galaxies

Y. Merckx,[a,*] **P. Correa,**[a,b] **K. D. de Vries,**[a] **K. Kotera,**[a,c] **G. C. Privon**[d,e,f] **and N. van Eijndhoven**[a]

[a] *Vrije Universiteit Brussel, Dienst ELEM, Pleinlaan 2, 1050 Brussels, Belgium*

[b] *Sorbonne Université, Université Paris Diderot, Sorbonne Paris Cité, CNRS, Laboratoire de Physique Nucleaire et de Hautes Energies (LPNHE), 4 place Jussieu, F-75252, Paris Cedex 5, France*

[c] *Sorbonne Université, CNRS, UMR 7095, Institut d'Astrophysique de Paris, 98 bis bd Arago, 75014 Paris, France*

[d] *National Radio Astronomy Observatory, 520 Edgemont Road, Charlottesville, VA 22903, USA*

[e] *Department of Astronomy, University of Florida, P.O. Box 112055, Gainesville, FL 32611, USA*

[f] *Department of Astronomy, University of Virginia, 530 McCormick Road, Charlottesville, VA 22904, USA*

E-mail: yarno.merckx@vub.be, pabcorcam@gmail.com, krijn.de.vries@vub.be, kotera@iap.fr, gprivon@nrao.edu, nick.van.eijndhoven@vub.be

We developed a framework for high-energy neutrino production in the dense central regions of starburst galaxies and apply it to (ultra)luminous infrared galaxies (U/LIRGs) in the Great Observatories All-Sky LIRG Survey (GOALS). First, we present results from our case study of the LIRG NGC 3690 (Arp 299, Mrk 171) which we compare to the current sensitivity of the IceCube Neutrino Observatory at the South Pole. Then, we make per-source flux predictions for all the U/LIRGs in GOALS. In particular, we conclude that our starburst-driven flux prediction cannot explain the neutrino flux recently observed by IceCube from the direction of the LIRG NGC 1068. This hints toward a non-starburst component, such as the active galactic nucleus in this galaxy, as the dominant source of the observed neutrinos. Last we use the per-source flux predictions to estimate the diffuse starburst-driven neutrino flux from the GOALS sample.

38th International Cosmic Ray Conference (ICRC2023)
26 July - 3 August, 2023
Nagoya, Japan

*Speaker

PoS(ICRC2023)972

1. Introduction

All-sky surveys at infrared (IR) wavelengths revealed the existence of galaxies which emit most of their bolometric luminosity ($L_{\rm bol}$) in the IR frequency range [1], such as Luminous Infrared Galaxies (LIRGs; $10^{11} L_\odot \leq L_{\rm IR} \equiv L_{\rm IR[8-1000\mu m]} < 10^{12} L_\odot$) and Ultraluminous Infrared Galaxies (ULIRGs; $L_{\rm IR} \geq 10^{12} L_\odot$). Locally, a substantial fraction of the LIRGs, and nearly all ULIRGs, are interacting gas-rich spiral galaxies [2]. Such interactions trigger dust-enshrouded starburst activity ($\sim$10$-$100 $M_\odot$ yr^{-1}) and Active Galactic Nuclei (AGN) in the central $\sim$100 pc of the interacting galaxies. The reprocessed emission from this starburst activity usually explains the extreme IR luminosity, but an additional contribution from reprocessed AGN radiation is possible [3]. Moreover, such starburst regions and AGN are promising hadronic accelerators, containing a merger-enhanced target density for the hadrons to interact with [4–6]. Inelastic collisions between accelerated hadrons and ambient radiation or baryonic matter yield mostly charged and neutral pions. The neutral pions decay to gamma rays while charged-pion decay yields high-energy neutrinos. The extreme IR emission in U/LIRGs, tracing enshrouded starburst activity and AGN, is therefore a possible tracer of high-energy neutrino production and hence also hadronic acceleration.

The IceCube Neutrino Observatory discovered astrophysical neutrinos in 2013 [7]. Despite the identification of the blazar TXS 0506+056 [8], the LIRG NGC 1068 [9], and the Galactic plane [10] as sources of high-energy neutrinos, the origin of the diffuse IceCube flux remains largely unknown. Motivated by the proximity, the enormous energy budget, and the potential relation between IR and neutrino luminosity, we investigate U/LIRGs as candidate neutrino sources. The IceCube Collaboration already sought for neutrinos from the ULIRG source population, but null results were reported [11]. Nevertheless, LIRGs have similar starburst properties as ULIRGs and appear to be $\sim$10$-$50 times more numerous than ULIRGs up to a redshift $z \sim 2$ [12]. Therefore, it is still valuable to investigate LIRGs as high-energy neutrino sources.

In this work we present a framework that relates the IR luminosity of a galaxy to the starburst-driven neutrino flux generated via proton-proton collisions and apply it to U/LIRGs in the Great Observatories All-Sky LIRG Survey (GOALS) [13]. This is a multi-wavelength survey targeting the nearest (redshift $z < 0.088$) and brightest U/LIRGs. GOALS is introduced in Section 2 and the framework is described in Section 3. In Section 4 we present the per-source and diffuse high-energy neutrino flux predictions for the GOALS sample obtained from our framework.

2. Great Observatories All-Sky LIRG Survey (GOALS)

The *Infrared Astronomical Satellite* (IRAS) performed the first all-sky survey at IR wavelengths [1]. Based on the obtained data, the IRAS Revised Bight Galaxy Sample (RBGS) was constructed. RBGS is a complete flux-limited sample of 629 galaxies with an IRAS 60-μm flux density $S_{60\mu\rm m,IRAS} > 5.24$ Jy and Galactic Latitude $|b| > 5^\circ$ [14]. Later, the GOALS sample was defined by selecting all objects in the RBGS with an IRAS luminosity of $L_{\rm IR,IRAS} \geq 10^{11} L_\odot$ [13]. The GOALS sample consists of 180 LIRGs and 22 ULIRGs within $z = 0.088$, which cover all galaxy-merger stages and also the full range of nuclear types, i.e. type-1 and type-2 AGN, LINERs, and pure starbursts. The GOALS collaboration characterizes a diversity of properties in this sample by making use of multi-wavelength data from ground-based and space-borne telescopes [15].

GOALS objects were originally defined from observations made with IRAS, which had a relatively poor angular resolution, i.e. between ~0.5' at 12 μm and ~2' at 100 μm [16]. The IRAS emission for a single GOALS object may therefore correspond to the cumulative emission of individual galaxies in an interacting system. However, we model starburst-driven neutrino production in the cores of U/LIRGs based on their EM emission (Section 3). As such, we require the IR luminosity per individual galaxy rather than the total IRAS IR luminosity of the system. For this reason, we use the IR luminosity obtained for 229 disentangled GOALS galaxies, derived from data obtained with the *Herschel Space Observatory* [3]. These 229 galaxies consist of 40 galaxies with $10^{10.08} L_\odot \leq L_{\rm IR} < 10^{11} L_\odot$, 167 galaxies with $10^{11} L_\odot \leq L_{\rm IR} < 10^{12} L_\odot$, and 22 galaxies with $L_{\rm IR} \geq 10^{12} L_\odot$. Figure 1 (left panel) shows the redshift distributions of the three galaxy groups.

These IR luminosities can contain a significant contribution from AGN activity. To correct for this, we use the average AGN contribution to the bolometric luminosity, $\langle \alpha_{\rm AGN} \rangle \in [0, 1]$, obtained by GOALS for the 229 galaxies [3]. The AGN-corrected IR luminosity ($L_{\rm IR,SB}$) is then obtained via $L_{\rm IR,SB} = (1 - \langle \alpha_{\rm AGN} \rangle) \cdot L_{\rm IR}$, which is justified as for U/LIRGs $L_{\rm bol} \sim L_{\rm IR}$ per definition [17]. Figure 1 (right panel) shows the distribution of the $\langle \alpha_{\rm AGN} \rangle$-values, which reflects that in the majority of the galaxies the AGN only has a secondary contribution to the bolometric luminosity. However, a fraction of the galaxies has a significant contribution from the AGN, i.e. ~14% has $\langle \alpha_{\rm AGN} \rangle > 0.2$ and ~3% has $\langle \alpha_{\rm AGN} \rangle > 0.5$ (AGN dominates over starburst). Moreover, one galaxy has $\langle \alpha_{\rm AGN} \rangle = 1$, which corresponds to the closest galaxy in the sample, NGC 1068. For the most nearby galaxies, however, the corresponding $\langle \alpha_{\rm AGN} \rangle$-values should be interpreted as upper limits [3]. Therefore, the $\langle \alpha_{\rm AGN} \rangle$-value of NGC 1068 is likely smaller than one.

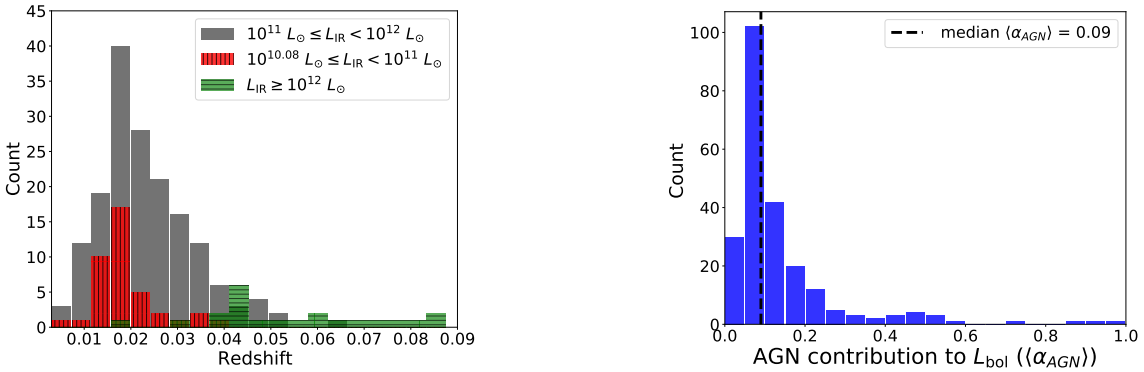

Figure 1: Left panel: Redshift distributions of the 229 targeted GOALS galaxies, consisting of 40 galaxies with $10^{10.08} L_\odot \leq L_{\rm IR} < 10^{11} L_\odot$, 167 galaxies with $10^{11} L_\odot \leq L_{\rm IR} < 10^{12} L_\odot$, and 22 galaxies with $L_{\rm IR} \geq 10^{12} L_\odot$ [3]. Right panel: Distribution of the average AGN contribution to the bolometric luminosity ($\langle \alpha_{\rm AGN} \rangle$) for the 229 disentangled GOALS galaxies targeted in this work. Figures taken from [18].

A fraction of the IR luminosity can be generated by starburst regions outside of the central ~100 pc. However, we only focus on the central region in our first approach as the interstellar medium (ISM) is sufficiently dense for efficient neutrino production. Therefore we introduce $\mathcal{G} \in [0, 1]$, which is the fraction between the IR luminosity generated by starburst activity in the nuclear region ($L_{\rm IR,nuclear}$) and the total starburst-driven IR luminosity ($L_{\rm IR,SB}$), i.e. $L_{\rm IR,nuclear} = \mathcal{G} \cdot L_{\rm IR,SB}$. This IR luminosity is used in the next section to estimate the starburst-driven neutrino flux.

3. The neutrino production model

Dynamical interactions between gas-rich galaxies allow for large amounts of dust and gas to be funneled from kpc-scales to the innermost ~100 pc. In this work we focus on this nuclear region and model it as a disk [19], parameterized by a radius ($R_{\rm SBR}$) and scale height ($H_{\rm SBR}$). As such the volume is computed as $V_{\rm SBR} = 2\pi R_{\rm SBR}^2 H_{\rm SBR}$ ([pc^3]). In this central region, stars are formed at an increased rate due to pressure waves induced by the interacting galaxies. The newly formed stars heat the thick layers of dust accumulated by active star formation, which re-radiate the energy in the IR regime. Furthermore, the massive stars with a mass $\gtrsim 8$ M$_\odot$ burn significantly faster through the hydrogen phase than low-mass stars and eventually explode as a core-collapse supernovae (CCSN). This implies a relation between the IR luminosity and supernova rate $\mathcal{R}_{\rm SN}$ ([yr^{-1}]),

$$\left(\frac{\mathcal{R}_{\rm SN}}{\rm yr^{-1}}\right) = \Lambda_{\rm IR} \cdot \left(\frac{\mathcal{G} \cdot [1 - \langle \alpha_{\rm AGN} \rangle] \cdot L_{\rm IR}}{\rm erg\ s^{-1}}\right). \tag{1}$$

Here $\Lambda_{\rm IR}$ is a calibration factor which is determined using the Starburst99 software [20]. Following our work in [18] we use $\Lambda_{\rm IR} = 5.97 \times 10^{-46}$ for further calculations.

In a supernova explosion the outer layer of the progenitor star is ejected with an energy of $E_{\rm SN}$~10^{51} erg. This drives strong shock waves in the surrounding medium which are capable of accelerating particles to high energies via diffuse shock acceleration. This could drive a rate of high-energy protons $Q_{\rm p}$ ([(GeV/c)$^{-3}$ cm^{-3} s^{-1}]) into the central nuclear disk. From diffusive shock acceleration we expect the distribution of high-energy particles to follow a power law, $Q_{\rm p} \propto p^{-\gamma_{\rm SN}}$, with p the particle momentum and $\gamma_{\rm SN}$ the spectral index. Theoretically we expect $\gamma_{\rm SN} = 4$ ($\gamma = \gamma_{\rm SN} - 2$ in energy space), but gamma-ray data requires softer spectra [21]. Additionally, we consider an exponential cutoff in the injection spectrum at the maximum achievable momentum $p_{\rm max}$ ([PeVc^{-1}]). For supernova-driven acceleration in a starburst region with an amplified magnetic field $p_{\rm max}$~1–100 PeVc^{-1} [5, 21]. Then the total injection rate of high-energy protons per unit volume due to all CCSN in the (circum-)nuclear starburst region is

$$Q_{\rm p} = \frac{N_C}{V_{\rm SBR}} \left[\frac{p}{m_{\rm p} c}\right]^{-\gamma_{\rm SN}} e^{\frac{-p}{p_{\rm max}}}. \tag{2}$$

where $m_{\rm p}$ is the proton mass and the normalization constant N_C is fixed by the total supernova-driven cosmic-ray (CR) luminosity ($\mathcal{L}_{\rm CR}$). The latter is estimated by converting a fraction $\eta_{\rm SN}$ of the kinetic energy released by the supernovae ($E_{\rm SN}$) into particle acceleration, i.e. $\mathcal{L}_{\rm CR} = \eta_{\rm SN} E_{\rm SN} \mathcal{R}_{\rm SN}$ ([erg yr^{-1}]). We take $\eta_{\rm SN} = 0.10$ [22] and we describe the normalization process in [18].

The accelerated protons can be injected into the dense and highly-pressurized ISM of the nuclear disk. Following [5], we assume a leaky-box model to describe the particle propagation in the central volume. The cosmic-ray momentum distribution function $\mathcal{F}(p)$ [(GeV/c)$^{-3}$ cm^{-3}] is then given by $\mathcal{F}(p) = Q_{\rm p} \cdot \tau$, with τ the average total time the CR spends in the central region. The latter is computed as $\tau = \left(\sum_i \tau_i^{-1}\right)^{-1}$, where i runs over all processes affecting particle propagation and τ_i^{-1} is the interaction probability of process i. In this work we consider particle advection by a galactic-scale outflow, which is common in starburst galaxies [23], and spatial diffusion as main processes of particle loss without secondary particle production. The advection timescale is estimated as $\tau_{\rm adv} \approx H_{\rm SBR}/v_{\rm adv}$, with an advection speed $v_{\rm adv}$~500–1500 km s^{-1} [18, 23]. The

timescale of spatial diffusion is estimated as $\tau_{\rm diff} \approx H_{\rm SBR}^2/D$, with D the diffusion coefficient which depends on the magnetic field strength (B) in the starburst region. Following [5], we use a Kolmogorov-type diffusion model. These particle losses are competing with proton-proton (pp) interactions, which is the only source of secondary particle production in our framework. The corresponding timescale is $\tau_{\rm pp} = (\xi c n \sigma_{\rm pp})^{-1}$, with $\xi \approx 0.5$ the inelasticity of the collision, c the speed of light, n~100−1000 cm^{-3} the nuclear ISM proton density, and $\sigma_{\rm pp}$ the cross section of inelastic pp-collisions [24]. Considering these processes, $\tau = [\tau_{\rm adv}^{-1} + \tau_{\rm diff}^{-1} + \tau_{\rm pp}^{-1}]^{-1}$.

Given the momentum distribution of accelerated particles $\mathcal{F}_{\rm p}$, the related energy distribution function is computed as $n_{\rm p} = 4\pi p^2 \mathcal{F}(p) {\rm d}p$ ([GeV^{-1} cm^{-3}]), which gives the available energy budget for high-energy neutrino production via pp-interactions. To relate the energy distribution of accelerated particles to the neutrino production rate q_ν ([GeV^{-1} cm^{-3} s^{-1}]), we use semi-analytical fits to neutrino spectra simulated with Monte Carlo generators in [24]. We describe this relation in more detail in [18]. Integrating this neutrino generation rate over the starburst volume gives the neutrino luminosity generated by that volume. As such, the all-flavour neutrino flux Φ_ν ([GeV^{-1} cm^{-2} s^{-1}]) expected from a source at luminosity distance D_L ([Mpc]) is then computed as

$$\Phi_\nu \left(E, \mathcal{R}_{\rm SN}, \gamma_{\rm SN}, p_{\rm max}, H_{\rm SBR}, v_{\rm adv}, n, B, D_L\right) = \frac{V_{\rm SBR}}{4\pi D_L^2} \cdot q_\nu \,, \tag{3}$$

using a particular diffusion model for the nuclear region and the supernova rate in the nuclear region computed as $\mathcal{R}_{\rm SN} = \mathcal{R}_{\rm SN}\left(L_{\rm IR}, \langle\alpha_{\rm AGN}\rangle, \mathcal{G}\right)$. As a result of neutrino oscillations and propagation over large distances, the single-flavour neutrino flux, Φ_{ν_j} with $j \in \{e, \mu, \tau\}$, is obtained by dividing the all-flavour neutrino flux by a factor of three [25].

4. Per-source and diffuse flux predictions for the GOALS sample

NGC 3690 (Arp 299, Mrk 171), shown in Figure 2, is a powerful intermediate-stage merger between two galaxies at $D_L \sim 50$ Mpc. We apply the framework described in Section 3 to the nuclear starburst region in the eastern galaxy, indicated with the letter A in Figure 2. In [18], we explain in detail how all the model parameters indicated in Eq. (3), except for $p_{\rm max}$, can be derived for this region from multi-wavelength data. Figure 2 (right panel) shows the neutrino flux predictions obtained from our model when using this multi-wavelength data as input. The corresponding values of the model parameters are also indicated in Figure 2. The orange double-dotted dashed lines show how the flux prediction is affected when the unknown parameter $p_{\rm max}$ is varied and the other parameters are kept constant. The isolated effect of changing the supernova rate is seen by comparing the orange double-dotted dashed line at 100 PeVc^{-1} to the blue solid line above. The supernova rate values correspond to the 1σ errors of a direct supernova-rate estimation for this galaxy [26]. Comparing the blue solid line to the black dotted line shows the isolated effect of changing the spectral index ($\gamma_{\rm SN}$) from a value based on gamma-ray data [27] to what is expected from diffuse shock acceleration, respectively. The red horizontal line shows the point-source sensitivity based on 10 years of IceCube data for an E^{-2} neutrino spectrum at the declination of NGC 3690 [28]. None of our predictions overshoot this sensitivity, which serves as a consistency check because NGC 3690 has not shown up as a significant neutrino emitter in previous IceCube analyses.

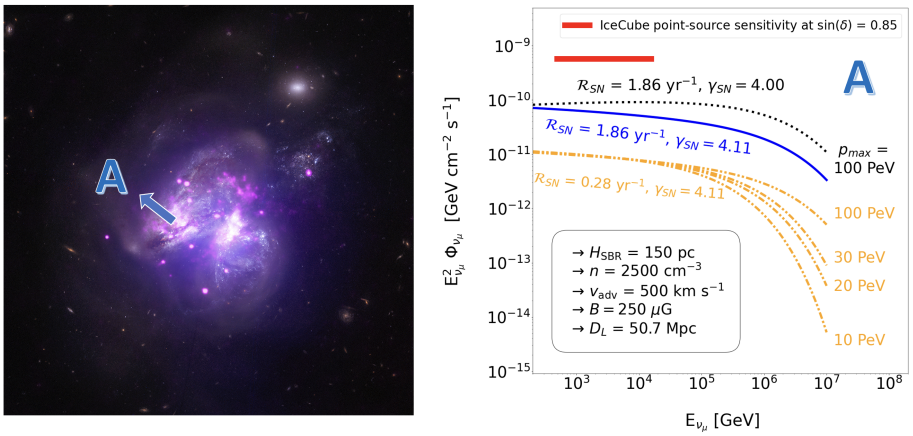

Figure 2: Left panel: Image of NGC 3690 showing both optical (white) and X-ray (pink) emission. Region A is a nuclear starburst region in the eastern galaxy [29]. This figure is edited from [30]. Right panel: Starburst-driven muon-neutrino flux as a function of energy obtained via our model. The red solid line is the IceCube point-source sensitivity for a source at the declination of NGC 3690 [28]. Figure edited from [18].

If all the parameters indicated in Eq. (3) are known for the $N = 229$ GOALS galaxies introduced in Section 2, then the corresponding per-source starburst-driven neutrino fluxes can be determined. Based on these values, the diffuse neutrino flux from the GOALS sample can be estimated as

$$\Phi_{\nu_\mu}^{\text{diffuse}}(E_{\nu_\mu}) = \frac{1}{4\pi} \sum_{i=1}^{N=229} \Phi_{i,\nu_\mu}(E_{\nu_\mu}) \, . \tag{4}$$

However, H_{SBR}, v_{adv}, B, and n the ISM proton density are unknown for the majority of these galaxies. As such, we opt to use the same values as found for our case study. Moreover, the spectral index γ_{SN} is unknown for nearly all GOALS galaxies. Therefore we fix the energy spectral index γ in all galaxies and investigate three different cases, i.e. $\gamma = \gamma_{\text{SN}} - 2 \in \{2, 2.25, 2.5\}$. The supernova rates are obtained via Eq. (1), using the IR luminosities and the average AGN contributions to the bolometric luminosity introduced in Section 2. Furthermore, we use $\mathcal{G} = 0.5$ for all galaxies. Finally, the luminosity distance to each of the galaxies is provided by GOALS [13]. Figure 3 (left panel) shows our per-source starburst-driven muon-neutrino flux predictions at 1 TeV ($\Phi_{i,\nu_\mu}^{1\text{TeV}}$) as a function of the declination (δ) of each of the investigated GOALS galaxies. The predictions are made for $\gamma = 2$ and the color scale indicates the $1-\langle\alpha_{\text{AGN}}\rangle$ value of the corresponding galaxy. For each object it is indicated whether it is a galaxy with $L_{\text{IR}} < 10^{11} L_\odot$, a LIRG, or an ULIRG. The three indicated galaxies are those with the strongest predicted starburst-driven neutrino flux. This assumes that $\langle\alpha_{\text{AGN}}\rangle = 1$ for NGC 1068 (see Section 2). However, for $\langle\alpha_{\text{AGN}}\rangle \leq 0.54$, NGC 1068 has the largest expected starburst-driven neutrino flux. In the most optimistic case, $\gamma = 2$ and $\langle\alpha_{\text{AGN}}\rangle = 0$, we find 2.44×10^{-13} TeV^{-1} cm^{-2} s^{-1} for NGC 1068. This prediction is about two orders of magnitude below the neutrino flux observed by IceCube from the direction of NGC 1068 [9]. Using our model, this hints towards a non-starburst component being the dominant source of neutrinos in this galaxy, such as AGN-related activity.

Figure 3 (right panel) shows the diffuse starburst-driven muon-neutrino flux for three spectral indices (γ_{SN}) calculated via Eq. (4) and using the same model parameter values as used in Figure

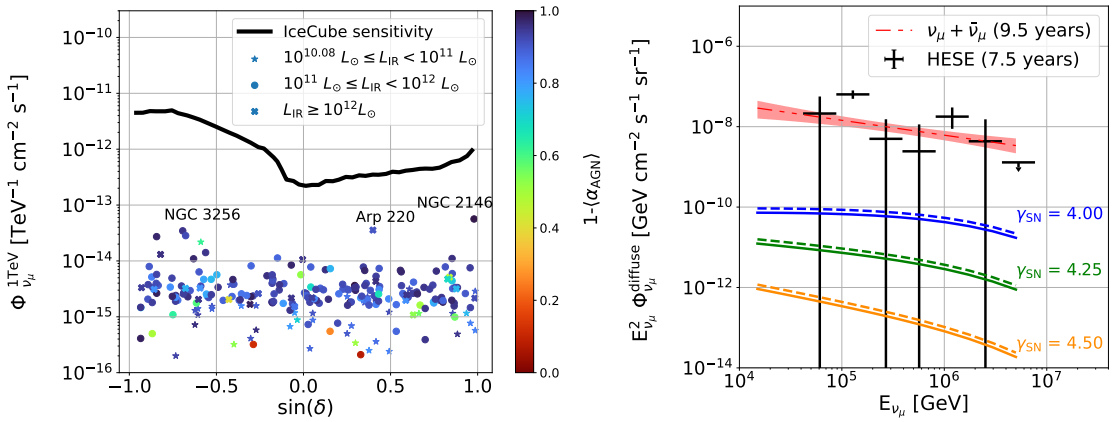

Figure 3: Left panel: Starburst-driven muon-neutrino flux at 1 TeV as a function of the declination of the GOALS galaxies. The color scale shows the $1-\langle\alpha_{\mathrm{AGN}}\rangle$ value of each galaxy and the black solid line indicates the IceCube point-source sensitivity [28]. For each galaxy we indicate whether it is a galaxy with $L_{\mathrm{IR}} < 10^{11}\ L_\odot$, a LIRG, or an ULIRG. Right panel: The diffuse starburst-driven muon-neutrino flux of the GOALS sample as a function of energy for three spectral indices. Per case the flux is estimated with (solid line) and without (dashed line) correcting for an AGN contribution to the IR luminosity. The flux predictions are compared to diffuse neutrino-flux measurements by IceCube [31, 32]. Figures taken from [18].

3 (left panel). Per spectral index, the diffuse flux is calculated both with (solid line) and without (dashed line) correcting for an AGN contribution to the IR luminosity. The black data points in Figure 3 (right panel) are the per-flavour IceCube measurements using the high-energy starting event (HESE) sample [31] and the red band is the best-fit unbroken power-law spectrum of astrophysical muon neutrinos observed by IceCube in the Northern Hemisphere [32]. All our flux predictions are well below the diffuse IceCube observations and our model is therefore not constrained by the IceCube measurements. However, as U/LIRGs show a positive redshift evolution [12], the contribution of the high-redshift counterparts should also be considered. This is usually done by extrapolating the cumulative neutrino flux from a local type of sources over cosmic history, where the assumption is made that the sources are standard-candle neutrino emitters [11]. For various reasons this extrapolation is complicated for LIRGs. First, the standard-candle assumption is highly unlikely as LIRGs show significant variations in nuclear activity among each other [18]. Second, we only considered starburst-driven neutrino emission from LIRGs while AGN in LIRGs are also promising neutrino sources. Last, high-redshift LIRGs evolve individually rather than in mergers [33] which could (significantly) affect the neutrino production efficiency. To properly estimate the diffuse flux prediction from the LIRG population these complications should first be investigated.

5. Conclusion

We presented a framework that relates the IR luminosity of a galaxy to the expected starburst-driven neutrino flux. We applied this framework in a case study to the LIRG NGC 3690 and used these results to make per-source neutrino flux predictions for the GOALS sample. None of the results exceed the point-source sensitivity of IceCube. Using our framework we concluded that our starburst-driven neutrino flux for NGC 1068 is well below the neutrino emission measured by IceCube from the direction of NGC 1068. Last, we used these predictions to estimate the diffuse starburst-driven neutrino flux of the GOALS sample. Our predictions are well below the diffuse

IceCube observations. However, we did not estimate the contribution of high-redshift U/LIRGs to the diffuse IceCube flux, which should be investigated in future studies.

Acknowledgments This work was supported by the Flemish Foundation for Scientific Research (1149122N, Y. M.), the European Unions Horizon 2020 research and innovation program (No 805486, K. D. de V.), the French National Research Agency (ANR-21-CE31-0025, P. C.), and the APACHE grant of the French Agence Nationale de la Recherche (ANR-16-CE31-0001, K. K.).

References

[1] G. Neugebauer *et al*, *ApJL* **278** (1984) L1.
[2] S. Stierwalt *et al*, *ApJS* **206** (2013) 1.
[3] T. Díaz-Santos *et al*, *ApJ* **846** (2017) 32.
[4] I. Tamborra, S. Ando and K. Murase, *JCAP* **2014** (2014) 043.
[5] E. Peretti *et al*, *MNRAS* **487** (2019) 168.
[6] K. Murase and F.W. Stecker, *arXiv e-prints* (2022) arXiv:2202.03381.
[7] IceCube Collaboration, M. G. Aartsen *et al*, *Science* **342** (2013) 1242856.
[8] IceCube Collaboration, M. G. Aartsen *et al*, *Science* **361** (2018) eaat1378.
[9] IceCube Collaboration, R. Abbasi *et al*, *Science* **378** (2022) 538.
[10] IceCube Collaboration, R. Abbasi *et al*, *Science* **380** (2023) 1338.
[11] IceCube Collaboration, R. Abbasi *et al*, *ApJ* **926** (2022) 59.
[12] B. Magnelli *et al*, *A&A* **553** (2013) A132.
[13] GOALS Collaboration, L. Armus *et al*, *PASP* **121** (2009) 559.
[14] D. B. Sanders *et al*, *AJ* **126** (2003) 1607.
[15] GOALS Collaboration. Available at: `goals.ipac.caltech.edu/`.
[16] *IRAS Catalogs and Atlases. Volume 1: Explanatory Supplement.*, vol. 1, Jan., 1988.
[17] V. U *et al*, *ApJS* **203** (2012) 9.
[18] Y. Merckx *et al*, *Phys. Rev. D* **108** (2023) 023015.
[19] A. M. Medling *et al*, *ApJ* **784** (2014) 70.
[20] L. Leitherer *et al*, *ApJS* **123** (1999) 3.
[21] P. Cristofari, *Universe* **7** (2021) 324.
[22] D. Caprioli and A. Spitkovsky, *ApJ* **783** (2014) 91.
[23] S. Veilleux *et al*, *A&AR* **28** (2020) 2.
[24] S. R. Kelner, F. A. Aharonian, and V. V. Bugayov, *Phys. Rev. D* **74** (2006) 034018.
[25] H. Athar, C.S. Kim and J. Lee, *Modern Physics Letters A* **21** (2006) 1049.
[26] M. Bondi *et al*, *A&A* **539** (2012) A134.
[27] M. Ajello, M. Di Mauro, V.S. Paliya and S. Garrappa, *ApJ* **894** (2020) 88.
[28] IceCube Collaboration, M. G. Aartsen *et al*, *Phys. Rev. Lett.* **124** (2020) 051103.
[29] R. D. Gehrz, R. A. Sramek and D. W. Weedman, *ApJ* **267** (1983) 551.
[30] Chandra X-ray Observatory. Available at: `chandra.harvard.edu/photo/2017/arp299/`.
[31] IceCube Collaboration, R. Abbasi *et al*, *Phys. Rev. D* **104** (2021) 022002.
[32] IceCube Collaboration, J. Stettner *et al*, *PoS* **ICRC2019** (2019) 1017.
[33] P. Madau and M. Dickinson, *ARA&A* **52** (2014) 415.

PoS(ICRC2023)972